Cellulose
https://doi.org/10.1007/s10570-023-05432-0

ORIGINAL RESEARCH

The effect of sulfate half-ester groups on the mechanical performance of cellulose nanocrystal-natural rubber composites

Iikpoemugh Elo Imiete · Luca Giannini · Luciano Tadiello · Marco Orlandi · Luca Zoia

Received: 23 September 2022 / Accepted: 1 August 2023

Abstract Cellulose nanocrystals (CNCs) are commercially produced *via* hydrolysis by sulfuric acid, resulting in the formation of sulfate half-ester groups on the surface of the nanoparticles. The sulfate half-esters promote good colloidal stability but could affect other properties of the CNCs. To study the impact of the sulfate half-ester groups on the mechanical properties of CNC-natural rubber composites, sodium hydroxide was used as a desulfation agent to partially remove this chemical functionality. Mechanical characterizations revealed that CNCs conferred outstanding mechanical properties to the composites. At the same time, differences in the amounts of sulfate half-ester groups had remarkable consequences for the tensile strength and the dynamic mechanical properties, while the vulcanization properties of the composites were less influenced.

Keywords Cellulose nanocrystal (CNC) · Sulfate half-ester · Desulfation · Composite · Natural rubber

Supplementary Information The online version contains supplementary material available at https://doi.org/10.1007/s10570-023-05432-0.

I. E. Imiete
MRT Department, Luxembourg Institute of Science and Technology, 41 rue du Brill, L-4422 Belvaux, Luxembourg

I. E. Imiete
Corimav Pirelli, Department of Material Science, University of Milano-Bicocca, Via R. Cozzi 55, 20125 Milan, Italy

L. Giannini · L. Tadiello
Pirelli Tyre S.p.A, Viale Sarca 222, 20126 Milan, Italy

M. Orlandi · L. Zoia (✉)
Department of Earth and Environmental Science, University of Milano-Bicocca, Piazza della Scienza, 1, 20126 Milano, Italy
e-mail: luca.zoia@unimib.it

Introduction

Tires facilitate the movement of goods and services and have been part of our society for decades. Demand is constantly increasing, and presently, the annual production of tires has exceeded 1.4 billion units (Sienkiewicz et al. 2012). A typical tire compound is made by dispersing fillers in a polymeric matrix, followed by the addition of processing aids, vulcanizing agents, and antidegradants. The addition of fillers primarily serves as a reinforcing agent and makes up roughly 28% of the tire compound (Rodgers and Waddell 2013; Danon and Görgens 2015), making them a crucial part of the tire industry. Carbon black and silica are the typical fillers used in the tire industry. Carbon black has been the preferred filler for decades, ensuring very interesting properties (Chollakup et al. 2021). However, due to the environmental concerns associated with carbon black and increasing regulations promoting the reduction of petroleum-derived materials, silica gradually became the

Published online: 09 August 2023

dominant component. Currently, tire compounds are prepared with dual fillers, comprising carbon black and silica. Since silica fillers are difficult to disperse in rubber matrixes, several types of highly dispersible silica have been developed. Their capabilities are still being explored to further reduce the use of carbon black. The silica production process is quite intensive, both mechanically and thermally, requiring a considerable amount of acids that generate a large amount of chemical waste (Haus et al. 2012; Fernandesa et al. 2018). Silica and carbon black both have relatively high densities, a fact that does not favor fuel efficiency (Bai and Li 2009). Going back to nature and identifying alternative materials that are widely available, light-weight, inexpensive, biodegradable, and renewable is a new priority and has evolved into a promising research area. In this context, the use of bio-based materials such as cellulose nanocrystals as a possible replacement of conventional fillers in rubber compounds would promote environmentally friendly tires.

roCellulose nanocrystals (CNCs), as well as cellulose nanofibers (CNFs), and nanocellulose (NC) are different terminologies that describe cellulose with various dimensions in the nanometer range. Several reviews about CNC extraction have been published (Habibi et al. 2010; Klemm et al. 2011; Moon et al. 2011; Ummartyotin and Manuspiya 2015; Jorfi and Foster 2015; Kim et al. 2015; Michelin et al. 2020). The production of CNCs can be carried out enzymatically or chemically using different types of enzymes and acids. In most cases, a combination of different acids is used to selectively hydrolyze the amorphous part of the fibers to obtain the nanocrystals. Sulfuric acid is by far the most widely used acid (Rajinipriya et al. 2018) to produce cellulose nanocrystals. The use of sulfuric acid for the hydrolysis generates, on the CNC surface, sulfate half-ester groups that confer colloidal stability to CNC suspensions (Eyley and Thielemans 2014). The role of these sulfate half-esters is important when CNCs are further processed for different applications (Colombo et al. 2015; Zoppe et al. 2015; Zoia et al. 2020; Llàcer Navarro et al. 2021). For example, it has been found that sulfate half-esters affect the thermal stability of CNCs (Roman and Winter 2004; Vanderfleet et al. 2019). Their presence has been suggested to promote dehydration reactions (Tang and Neill 2007). This latter aspect poses a challenge when CNCs are used for composites (Dufresne 2012, 2017), where the processing could require high temperatures, such as melt mixing (Gan et al. 2020). Although several publications are showing improved thermal properties of CNCs exposing higher levels of sulfate groups (Voronova et al. 2013; Zhao et al. 2015), further studies are necessary to understand their effect on other performances. Beside concerns regarding the thermal stability of CNCs, the partial consumption of the hydroxyl groups by the sulfate esters, at which coupling reactions take place during composite processing, could influence the surface chemistry of CNCs, affecting as such the final performances of the composite (Lin and Dufresne 2014). Additionally, the interactions between the filler and the rubber are probably influenced as well (Cao et al. 2013). The properties of CNCs at different sulfate half-ester concentrations have been studied by applying desulfation or sulfation reactions (Jordan et al. 2019); however, the impact of gradually changing amounts of sulfate esters on CNC surfaces has not been investigated on composites.

In this work, cellulose nanocrystals were gradually desulfated with an aqueous NaOH solution. The partially desulfated CNCs exhibiting different concentrations of sulfate half-esters were used to make a composite with natural rubber using silanes as a compatibilising agent. The mechanical properties conferred to the composites at various concentrations of sulfate esters were compared with a solely silica-reinforced compound as a reference.

Materials and methods

Materials

A water suspension of cellulose nanocrystals (11.5–12.5% (w/w)) was purchased from CelluForce (Canada). Highly dispersible silica Ultrasil VN3 was obtained from Evonik (Germany), soluble sulphur and *N*-cyclohexyl-2-benzothiazylsulfenamide (CBS) from Zolfoindustria (Italy), zinc oxide (ZnO) from Zincolossidi (Italy), stearic acid from Sogis (Italy), and 2,2,4-trimethyl-1,2-dihydroquinoline (TMQ) from Sovchem (UK). *N*-(1,3-Dimethylbutyl)-*N*'-phenyl-*p*-phenylenediamine (6PPD) was obtained from Eastman (US). Von Bundt (Thailand) supplied high-ammonia natural rubber latex with solid contents of

60% (w/w). Sodium hydroxide (NaOH), acetic acid, bis(triethoxysilylpropyl)disulfide (TESPD), and 3-aminopropyltriethoxysilane (APS) were purchased from Merck Sigma-Aldrich (Germany).

Desulfation procedure

The desulfation procedure followed the method described by Hasani et al. (Hasani et al. 2008) with little modification. The procedure has been optimized at small scale (1 g of CNCs), before a large-scale reaction was performed twice for composite preparation. In brief, an equal amount of freeze-dried CNCs (20 g) was dispersed in 300 mL of water with sodium hydroxide (NaOH) at concentrations of 0.3, 0.6, and 1.2 M. The various samples were stirred while being heated in an oil bath at 65 °C for 3 h. Thereafter, the reaction was stopped by pouring cold water into the reaction mixture. The work-up was achieved by dialyzing for several days until a neutral pH of the washings was obtained. The suspension was removed from the dialysis tubes and transferred to a beaker to be concentrated. All samples were concentrated at 100 °C until the samples attained a 9–10% (w/w) for co-precipitation.

Preparation of composites

CNC suspensions were mixed with natural rubber latex to prepare a series of 30 PHR (parts per hundred rubber) masterbatch composites. The mixtures were continuously stirred for several minutes until good homogeneity was achieved. Coagulation was then achieved by the dropwise addition of acetic acid. The CNC/NR coagulates were chopped into small pieces, soaked in water overnight, and dried in an oven at 40 °C until constant weight. The final compounds were made by melt mixing the coagulates in a Brabender internal mixer (chamber volume 50 mL, 0.9 fill factor) with the addition of processing aids, coupling and vulcanizing agents. While compounds made of CNCs were coagulated with natural rubber, the reference (S-TESPD) compounds were prepared by compounding silica, dried natural rubber, and other materials provided in the recipe. All the compounding procedures were performed twice. The recipes are reported in Table 1, while the mixing procedure is reported in Table 2.

Table 1 Formulation recipes for reference silica compounds with TESPD silane (S-TESPD), and desulfated CNC compounds prepared with TESPD silane (CNC-TESPD) and APS silanes (CNC-APS)

Materials (PHR)	S-TESPD	CNC-TESPD	CNC-APS
Natural rubber (NR)	100		
Silica	30		
NR/CNC masterbatch		130	130
TESPD	2.4	2.4	
APS			2.4
Sulphur	2	2	2
Zinc oxide	5	5	5
Stearic acid	2	2	2
CBS	2	2	2
TMQ	1	1	1
6PPD	1.5	1.5	1.5

*PHR – parts per hundred rubber

Characterizations of CNCs

Particle sizes and surface charges of desulfated CNCs were estimated by dynamic light scattering and zeta potential measurements, respectively. Both measurements were conducted on a Malvern Zetasizer, Malvern (UK), at a scattering angle of 90°. The data were calculated as the average of three measurements, with each measurement being comprised of 30–50 sub-runs. The elemental content before and after desulfation was estimated by elemental analysis using a CHNS/O Series II analyser from PerkinElmer (US) and cysteine as a calibration standard. The crystalline arrangements within CNCs were studied with an X`Pert PRO diffractometer from PANalytical Company, using Cu Kα (1.54 Å) as an X-ray source. The operating voltage and the current were kept at 40 kV and 30 mA, respectively. Fourier Transform Infrared Spectroscopy with Attenuated Total Reflectance (FTIR-ATR) was used to record spectra on a Nicolet iS10 IR spectrometer, Thermo Scientific (US) equipped with a diamond ATR Smart device, applying 32 scans, covering a wavenumber range of 4000–800 cm^{-1}, with a resolution of 1 cm^{-1}). Surface morphology and dimensions were investigated by Field Emission Scanning Electron Microscopy (FESEM). The samples were prepared for this by dispersing a small amount of CNCs in ethanol and sonicating the suspension for 15 min. A drop of the suspension was then placed on a silicon substrate and

Table 2 Mixing procedure for references and CNC compounds

Mixing stage	Time (min)	Temperature (°C)	Activity
Step 1	0	130	Load CNC/NR masterbatches or rubber and silica filler
	2		Add silanes
	6		Add stearic acid
	7		Unload
Step 2	0	60	Load masterbatches step 1
	1		Add sulphur, CBS, TMQ, 6PPD, ZnO
	3		Unload

dried in the air. The FESEM analysis was performed using a Zeiss UltraPlus FESEM, Zeiss (Germany), operating at 5.0 kV and a working distance between 3.5 and 4 mm. To overcome the drawback of the non-conductive nature of CNCs, a 5–7 nm layer of carbon was spattered on the surface before image acquisition. Thermal Gravimetric analysis (TGA) was performed using a Mettler Toledo TGA1 instrument, Mettler Toledo (US). A few milligrams of the sample were placed in an open crucible pan and heated from 30 to 600 °C in a nitrogen atmosphere with a flow rate of 50 mL/min while the heating rate was 20 °C/min.

Characterization of rubber compounds

The vulcanization kinetics of the compounds were recorded using a Moving Die Rheometer RPA 2000, Alpha Technologies (US). The measurements were performed at a temperature of 150 °C, at a pressure of 4.3 bar, and with a rotor frequency of 1 Hz for a run time of 30 min. From the measurement, the minimum (ML) and maximum torque (MH), their difference (ΔM), scorch time (TS2), cure rate index (CRI), and optimum cure time (T90) were determined. Dynamic mechanical analyses of both unvulcanized and vulcanized compounds were performed using the Rubber Process Analyzer RPA 2000, Alpha Technologies (US), working in the shear stress mode. The strain sweep measurements were performed from 1 to 100% strain at 70 °C and a frequency of 1 Hz. Vulcanized samples were pressed into 2 mm-thick sheets by a two-roll mill and vulcanized in a hydraulic press under a pressure of 4.3 bars at 150 °C for 30 min. The vulcanized samples were conditioned in the measuring environment for 24 h. Samples for tensile mechanical analyses were prepared by die-cutting the vulcanized sheets into five dumbbell-shaped specimens of standard dimensions. The measurements were performed according to ISO 37 and UNI 6065 standards by using a Zwick/Roell tensile testing machine (Italy). The stress-strain curves were recorded by progressive straining of the samples. The reported data represent the mean and the standard errors resulting from three independent analyses.

Results and discussions

Characterizations of CNCs

Table 3 presents the findings of characterizations demonstrating the characteristics of cellulose nanocrystals before and after desulfation reactions at a large scale, using 20 g of CNCs.

Table 3, column 1, reports the dimensions of pristine CNCs and CNCs treated with NaOH at various concentrations, measured by dynamic light scattering (DLS). The DLS method estimates the hydrodynamic diameter of spherical particles undergoing Brownian motion. The diameter of spherical particles does

Table 3 Particle size, zeta potential, sulfur content, and crystallinity index of pristine cellulose nanocrystals (CNCs) and CNCs desulfated using aqueous NaOH at 0.3, 0.6, and 1.2 M concentrations

Sample	Size (nm)	Zeta potential (− mV)	Sulfur (%)	CI (%)
CNC	105 ± 10	− 50.9 ± 2.3	2.05	86.3
0.3	198 ± 19	− 35.5 ± 1.5	1.86	83.4
0.6	240 ± 22	− 32.1 ± 1.4	1.71	77.8
1.2	260 ± 23	− 27.7 ± 1.7	1.66	72.2

not accurately correlate to the rod-like structure of CNCs due to the geometric differences. Therefore, the estimations made with DLS are observed to be around half as long as those made with SEM, TEM, and AFM and are meant to be used for comparative analyses (Boluk and Danumah 2014). The size of the CNC particles before desulfation was estimated to be 105 nm, but after treatment with soda solutions of increasing concentration during the desulfation process, the diameters grew, reaching a particle size of 260 nm at a soda concentration of 1.2 M (sample 1.2). This increase is in contrast to literature reports (Lin and Dufresne 2014) and can be explained by possible aggregation phenomena of the particles due to the removal of the sulfate groups.

CNCs produced with sulfuric acid maintain good colloidal stability in suspension due to the electrostatic repulsion of the negative surface sulfate half-ester groups. The zeta potential (Table 3, column 2) shows a clear trend. CNC suspensions before desulfation measured up to −50.9 mV. Similarly high zeta potentials of CNC suspensions have been reported elsewhere for the sulphuric acid hydrolysis of filter paper with −52 to − 58 mV (Boluk and Danumah 2014) and −78.3 mV obtained from the sulphuric acid hydrolysis of microfibrillated cellulose (Börjesson et al. 2018). The sample with the lowest zeta potential in this work results from the treatment with 1.2 M sodium hydroxide. This implies that more sulfate half-esters were removed from the surface of the particles, lowering consequently the zeta potential (Lin and Dufresne 2014). For suspensions stabilized by electrostatic repulsions, the minimum zeta potential required to maintain colloidal stability is ±30 mV (Jacobs and Müller 2002); however, large zeta potentials do not always guarantee stability as agglomeration can occur due to van der Waals-type attractive forces (Bhattacharjee 2016; Beyene et al. 2018). The colloidal stability obtained at the higher level of desulfation was, however, considered sufficient for composite preparation through co-precipitation.

Elemental analysis and conductometric titration are widely used methods employed to determine the amount of grafted sulfate groups (Gu et al. 2013), with the first method resulting in higher total sulfur concentrations than the second (Dong et al. 1998). The sulfate half-ester content of the various desulfated CNCs was estimated in this work by elemental analysis. The data are presented in Table 3, column 3. Sulfur content was 2.05% before desulfation and decreased to 1.66% for sample 1.2. The trend reported in Table 3 is a consequence of desulfation and is in agreement with the zeta potential analyses and literature reports (Lin and Dufresne 2014). For decades, mercerization by treating cellulose with sodium hydroxide has been used in the textile industry to swell cellulose, and it has been adopted to activate cellulose for further reactions (Dinand et al. 2002; Mansikkamäki et al. 2007; Duchemin 2015). These conditions could not be applied in this work since the original morphology and structure of the surfaces of CNCs had to be maintained after desulfation reactions. Therefore, the alkaline conditions were selected in order to avoid the transformation of cellulose type I to type II (Lin and Dufresne 2014). X-ray diffraction was used to confirm morphological integrity and study the impact of the treatment on the crystallinity of the fibers. The results are shown in Fig. 1. The crystalline peaks of the various samples were found along the 2θ planes of 12.3, 14.9, 16.5, 20.5, 22.7 and 34.5°. Peaks observed at 2θ = 14.9, 16.5, 22.7, and 34.5° correspond to the planes of (1 0), (1 1 0), (2 0 0) and (0 0 4) of the cellulose $I_{\beta;}$ peaks observed at 12.3 and 20.5° correspond to cellulose II (Cheng et al. 2011; Gong et al. 2017), which is more stable than native cellulose I and is typical of commercial CNCs having portions of both type I and type II. As seen in the various peaks, the impact of the desulfation process led to a limited conversion of the material to cellulose II.

The crystallinity index of the various samples was estimated by the deconvolutional method (Figure S1) using a Gaussian distribution to deduce the ratio of the crystalline regions to the amorphous ones (Park et al. 2010; Rambo and Ferreira 2015; Rongpipi et al. 2019; Yao et al. 2020). As shown in Table 3, column 4, the crystallinity index decreased from 86.3% for pristine CNCs (86.3%) to 72.2% for sample 1.2, and it was concluded that the NaOH treatment partially affected the crystallinity of CNCs. To further prove the reliability of the gradiented desulfation treatments for CNCs, FTIR-ATR spectra were acquired for all samples. Figure 1, on the right, shows FT-IR spectra (1150–900 cm^{-1}) with a band at 1033 cm^{-1} attributable to the stretching vibration of sulfate half-ester groups (Lin and Dufresne 2014). In comparison with pristine cellulose nanocrystals, the intensity of this peak gradually decreased from sample 0.3 to sample

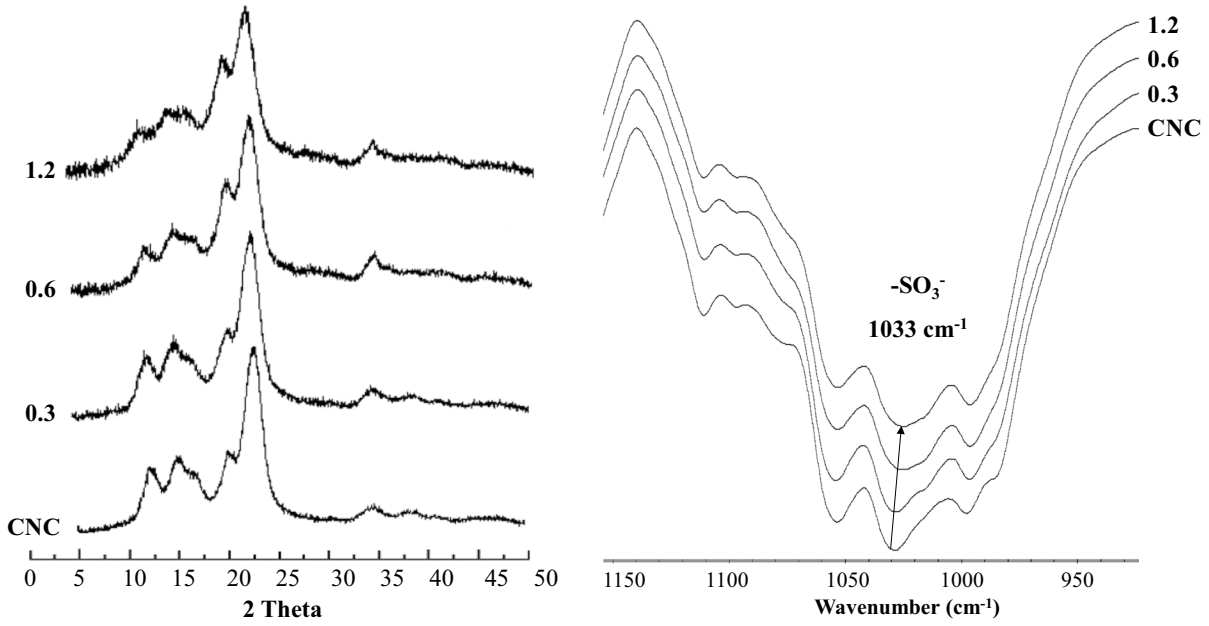

Fig. 1 X-ray diffraction patterns and FT-IR spectra (1150–900 cm^{-1}) of pristine cellulose nanocrystals (CNCs) and CNCs desulfated using aqueous NaOH at 0.3, 0.6, and 1.2 M concentrations

1.2, indicating a decrease in the gradient contents of sulfate groups on the surface of the CNC samples. Derivative and thermogravimetric analyses of cellulose nanocrystals before and after desulfation are presented in Fig. 2. The onset of weight loss at the first stage was attributed to possible adsorbed water and organics and reached a maximum at 42 °C for all samples except sample 1.2 (57 °C). The evolution of the degradation at the second stage showed similar degradation kinetics starting around 250 °C. This stage is recognized to be related to the sulfate half-ester hydrolysis (Roman and Winter 2004; Börjesson et al. 2018; Gan et al. 2020). By increasing the NaOH concentration for the treatments, the intensity

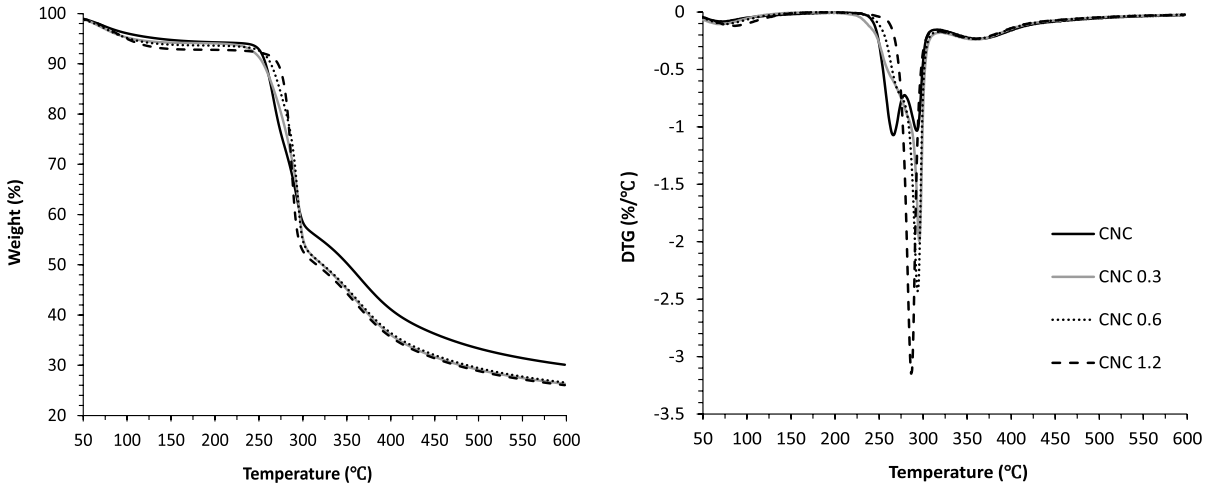

Fig. 2 Thermogravimetric and derivative curves of pristine cellulose nanocrystals (CNCs) and CNCs desulfated using aqueous NaOH at 0.3, 0.6, and 1.2 M concentrations

of the peak related to the second stage decreased, in agreement with the removal of superficial sulfate half-esters.

The morphology of pristine and desulfated cellulose nanocrystals was additionally studied with scanning electron microscopy imaging (Fig. 3). Pristine cellulose nanocrystals are rod- or needle-like in shape, and the fibers maintain a three-dimensional network. Desulfated CNCs still largely have a rod-like shape, although there are some noticeable changes.

Samples were prepared at the same concentration ranges; however, sample 1.2 showed more CNC aggregation, causing them to appear as fused particles. Despite the large extent of the desulfation in this sample, the morphology of the pristine CNCs was maintained. The other desulfated samples show strands of CNC particles with minimal aggregations.

Characterization of rubber compounds

Vulcanization properties

Vulcanization studies were conducted on the compounds made with pristine cellulose nanocrystals and the samples treated at different NaOH concentrations to evaluate the effect of the sulfate half-esters on the vulcanization properties. The various rubber compounds were prepared using APS and TESPD silanes as compatibilizers, and the vulcanization kinetics were studied at 150 °C. Table 4 reports the vulcanization properties compared to the silica compound as a technological reference. The data reported are the average of two experiments with their respective standard deviations. The vulcanization trends were heavily influenced by the compatibilising silanes. APS samples showed an early optimum curing time and higher cure rate index (CRI) compared with TESPD compatibilized compounds, due to the accelerating effect of APS on sulfur curing (Mostoni et al. 2021).

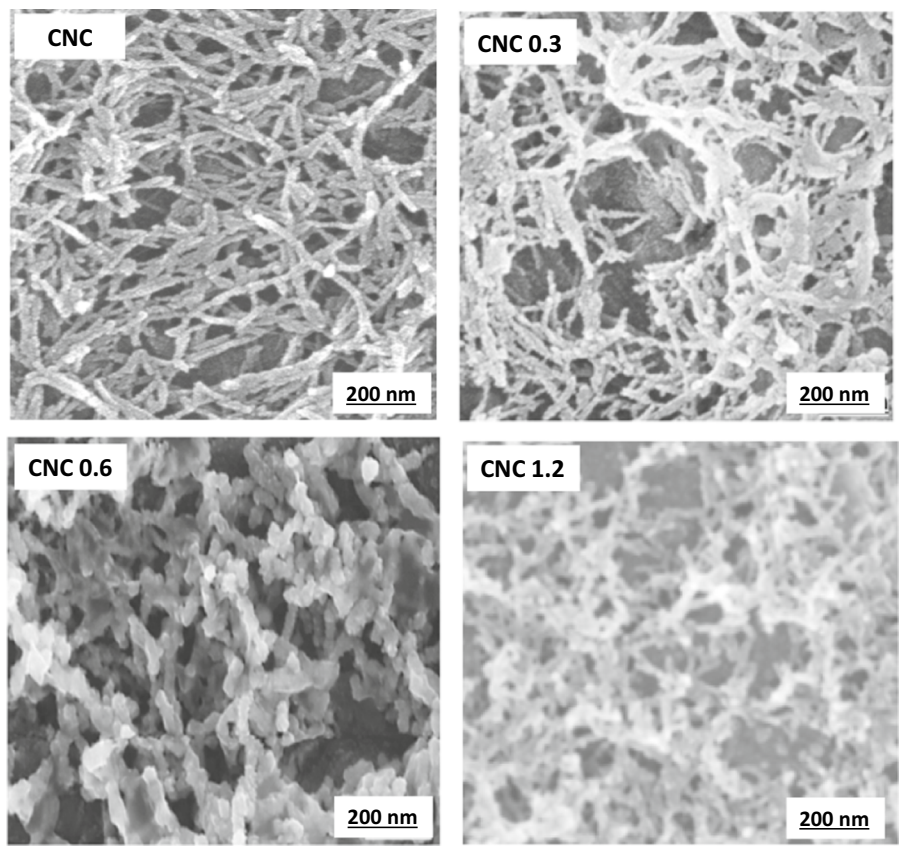

Fig. 3 SEM images of pristine cellulose nanocrystals (CNCs) and CNCs desulfated using aqueous NaOH at 0.3, 0.6, and 1.2 M concentration

Table 4 Vulcanization kinetics of pristine and desulfated CNC-containing compounds compatibilized with APS and TESPD silanes. A silica compound compatibilized with TESPD is used as reference

Parameter	APS compatibilized compounds				TESPD compatibilized compounds				
	CNC	0.3	0.6	1.2	Silica	CNC	0.3	0.6	1.2
TS2 (min)	3.1 ± 0.3	2.9 ± 0.2	2.8 ± 0.3	2.5 ± 0.2	9.7 ± 0.4	8.5 ± 0.7	5.3 ± 1.2	5.1 ± 0.6	5.4 ± 0.4
T90 (min)	5.6 ± 0.7	5.4 ± 0.6	5.3 ± 0.7	4.7 ± 0.9	15.7 ± 2.0	14.3 ± 1.2	9.5 ± 1.0	9.3 ± 1.0	9.5 ± 0.8
CRI (min^{-1})	39.7 ± 5.0	40.8 ± 3.1	40.0 ± 3.0	45.5 ± 3.2	20.0 ± 1.5	17.1 ± 2.1	24.0 ± 2.0	29.9 ± 1.9	24.3 ± 1.7
ML (dNm)	2.3 ± 0.2	1.9 ± 0.2	2.1 ± 0.1	1.8 ± 0.2	1.6 ± 0.1	1.7 ± 0.2	1.6 ± 0.2	1.9 ± 0.2	1.6 ± 0.1
MH (dNm)	19.0 ± 2.0	15.5 ± 1.5	15.4 ± 1.5	15.5 ± 2.0	12.3 ± 1.2	14.4 ± 1.5	15.1 ± 2.3	15.7 ± 1.1	14.2 ± 1.4
ΔM (dNm)	16.7 ± 1.7	13.5 ± 1.8	13.2 ± 1.3	13.7 ± 1.1	10.7 ± 1.0	12.6 ± 1.0	13.5 ± 1.6	13.8 ± 1.1	12.6 ± 2.0

In this regard, the different amounts of sulfate groups present on the CNC surfaces had a minimal influence on the vulcanization process (TS2, T90, and CRI) when compounded with APS, as the properties of sample 1.2 were similar to those of the other samples. Significant differences were observed on the torque values ML, indicative of the physical interactions on the compound, and MH, indicative of the cross-linking density. APS compatibilized compounds containing CNCs that were treated with aqueous NaOH exhibited lower torque values due to the reduction of the cross-linking during the vulcanization process as a consequence of the removal of sulfate groups. In this case, the possible interaction between the sulfate group of CNCs and the amine group of APS could play an important role during the surface functionalization.

The compounds compatibilized with TESPD silanes showed a similar trend: the kinetic rate slightly increased with the decrease in sulfate groups. Interestingly, an opposite trend with respect to APS was observed regarding the torque values ML and MH. The use of NaOH-treated CNCs led to similar or even higher values compared to the use of pristine CNCs for the TESPD compatibilized compounds. This was probably due to the increased availability of hydroxyl groups on the CNC surface as a consequence of the desulfation reaction, which provided more active sites for the coupling reaction with the TESPD silanes and more efficient filler-rubber interactions. Comparatively, the pristine and desulfated CNC compounds showed better vulcanization properties compared to the reference silica compound. Despite minimal differences in the vulcanization kinetics between the pristine and desulfated CNCs, the sulfate groups were not observed to play a remarkable role on the curing kinetics. In general, the results have shown that desulfation treatment of CNCs with aqueous NaOH at concentrations below 1.2 M would not significantly interfere with the vulcanization kinetics. The previous observation of acidic groups interfering with the vulcanization mechanism (Yasir et al. 2015) was not confirmed.

Dynamic mechanical properties

The dynamic mechanical analyses of the CNC/rubber compounds were performed in shear stress mode after vulcanization. The reinforcement of the pristine and desulfated cellulose nanocrystals was studied and compared with silica-reinforced compounds, and the results are shown in Table 5. For the APS silanized compounds, the storage modulus of the compound reinforced with pristine cellulose nanocrystals was 30% higher than that found for the reference silica. This reinforcing effect is a result of the inherent stiffness and reinforcing morphology of the cellulose nanocrystals. A high Payne effect, measured as the difference between the low and high strain modulus, ΔG', and a high tangent delta (tanδ) value, were detected. The Payne effect is indicative of the filler network breakdown, while the tanδ displays the synergistic effect of the elastic and inelastic portions of the compounds. Extremely high tanδ values are generally related to high rolling resistance and higher fuel consumption; values that tend towards zero are desirable. The use of desulfated CNCs caused a reduction in the storage modulus G'_0 when compared to the use of pristine CNCs, while G'_∞ was only marginally affected. The low G'_0 and relatively high G'_∞ at low half-ester sulfate group content highlighted the role of the CNCs in the compounds. The rod-like structure of

Table 5 Storage moduli of pristine and desulfated CNC compounds compatibilized with APS and TESPD silanes. A silica compound compatibilized with TESPD is used as a reference

Parameter	APS compatibilized compounds				TESPD compatibilized compounds				
	CNC	0.3	0.6	1.2	Silica	CNC	0.3	0.6	1.2
G'_0(kPa)	1430 ± 118	1100 ± 99	1120 ± 101	1054 ± 95	1075 ± 97	1330 ± 120	1075 ± 97	1160 ± 104	975 ± 92
G'_∞(kPa)	869 ± 74	770 ± 69	798 ± 72	800 ± 78	705 ± 62	816 ± 73	751 ± 74	752 ± 67	693 ± 71
ΔG' (kPa)	561	330	322	254	370	514	324	408	282
$\tan\delta_0$	0.030	0.029	0.030	0.021	0.033	0.052	0.037	0.036	0.026
$\tan\delta_\infty$	0.062	0.061	0.059	0.055	0.048	0.058	0.06	0.065	0.055

CNCs contributed to a strong filler-filler network that was rigid enough to resist deformation at low cyclic solicitations. The relatively high storage modulus G'_∞ at low sulfate ester groups has been partly attributed to the increased availability of hydroxyl groups resulting from the desulfation process, and partly to more efficient filler-rubber interactions. The improved interactions between desulfated CNCs and rubber matrix most likely reduced the breakdown of the filler network. As a result, the Payne effect and tanδ values were lower compared to the pristine cellulose nanocrystals and more similar to the technological silica reference.

The storage modulus of the compounds compatibilized with TESPD silanes also showed a similar trend. The higher storage modulus was observed with pristine CNCs. After treatment with aqueous NaOH, the storage modulus G'_0 decreased roughly with increasing NaOH concentrations. This could also be explained by the reduction of filler-filler interactions promoted by the high polar sulfate groups. Again, it was possible to observe the same trend for the Payne effect and tanδ values. When compared to the prepared silica compound, CNC compounds compatibilized with TESPD exhibited higher tanδ values with respect to desulfated CNC compounds compatibilized with TESPD. The effect, however, appeared less pronounced when compared with the APS compatibilization series, where the possible interaction between the sulfate groups of CNCs and the amine groups of the APS generated a remarkable effect.

Tensile properties

The tensile properties of pristine and desulfated CNC compounds prepared with APS and TESPD are presented in Table 6, along with data for a compound containing silica as a technological reference. The tensile properties of the CNC compounds showed remarkable properties, always higher than the reference silica. The unmodified CNC reference compounds, i.e., both the APS and the TESPD compatibilized samples, show high stiffness but reduced properties at break. In particular, the compounds compatibilized with APS were unable to be stressed up to 300% and the tensile strength was poor. This could be a result of brittleness in the compounds. A 300% stress is vital for tire testing and applications, and the brittleness of this compound may not be suitable. As already highlighted, it is possible that electrostatic interactions between sulfate groups and the amine moieties in APS-silanized compounds contribute to such stiffness. It is known that not all the immobility of polymeric chains is caused by covalent bonds. This type of interaction can cause restrictions in polymer chains, thereby making them tend towards a glassy behavior (Fukahori 2005; Montes et al. 2010; Choi and Ko 2014).

Considering the need to improve the tensile strength of CNC compounds, the partial removal of half-sulfate esters seemed to be a promising approach: samples 0.3 and 0.6 presented the best properties at break. Those data were also indicative of a good filler dispersion, assured by a relatively good colloidal stability, as highlighted in Table 3. Incorporating CNCs treated with a 1.2 M aqueous NaOH solution made the compound brittle again, and it could be hypothesized that the filler aggregation phenomenon became more important and detrimental. Despite the benefits associated with the reduction of sulfate esters, it seemed that a threshold existed for the degree of desulfation to be useful. For TESPD silanized compounds, the tensile strength of desulfated compounds showed more constant values. This also alluded to a

Table 6 Tensile properties of pristine and desulfated CNC compounds compatibilized with APS and TESPD silanes. A silica compound compatibilized with TESPD is used as a reference

Parameter	APS compatibilized compounds				TESPD compatibilized compounds				
	CNC	0.3	0.6	1.2	Silica	CNC	0.3	0.6	1.2
10% stress (MPa)	0.71 ± 0.04	0.48 ± 0.02	0.51 ± 0.03	0.48 ± 0.02	0.38 ± 0.03	0.68 ± 0.02	0.48 ± 0.03	0.54 ± 0.03	0.47 ± 0.03
50% stress (MPa)	3.30 ± 0.2	1.63 ± 0.1	1.79 ± 0.1	1.84 ± 0.2	1.08 ± 0.1	2.57 ± 0.3	1.58 ± 0.2	1.73 ± 0.2	1.64 ± 0.2
100% stress (MPa)	7.76 ± 0.4	3.60 ± 0.2	3.71 ± 0.2	4.34 ± 0.3	1.91 ± 0.2	5.54 ± 0.3	3.29 ± 0.2	3.44 ± 0.2	3.59 ± 0.2
300% stress (MPa)	–	14.93 ± 0.8	15.66 ± 0.8	–	10.02 ± 0.6	15.87 ± 0.8	13.07 ± 0.7	12.98 ± 0.7	13.87 ± 0.7
Elongation at break (%)	157 ± 8	354 ± 18	398 ± 20	269 ± 14	387 ± 20	352 ± 18	395 ± 20	413 ± 21	349 ± 18
Tensile strength (MPa)	12.3 ± 0.6	19.5 ± 1.0	22.5 ± 1.1	13.9 ± 0.7	16.2 ± 0.9	17.9 ± 0.9	18.1 ± 0.9	20.1 ± 1.0	17.2 ± 0.8

generally improved filler-matrix interaction brought about by the desulfation. The values from 10 to 300% elongation and elongation at break were also noticed to be higher than the referenced silica, and these samples showed a combination of properties of being strong, stiff, and tough.

Conclusions

Cellulose nanocrystals are widely produced with sulphuric acid, which grafts on the surface sulfate half-ester groups. Pristine CNC compounds showed outstanding mechanical properties, even if some parameters, such as tanδ, indicated a high rolling resistance. The objective of this study was to investigate how the content of sulfate half-ester groups exposed on the surface of CNCs affects the mechanical properties of CNC/natural rubber composites. Through the regulation of reactant ratios and subsequent desulfation, gradually changing contents of sulfate groups can be achieved on the surface of CNCs. Composites were prepared with the various desulfated CNCs and compatibilized with APS and TESPD silanes. The properties of the composites were relatively indicative of the degree of desulfation. The highly desulfated samples showed a reduction in crystallinity; however, it was observed that the removal of the sulfate groups provided some improvements in the compound's mechanical properties, especially the tensile strengths. The main advantages were observed in the tanδ values, which clearly indicated that desulfated CNC compounds are characterized by lower rolling resistance. This indicates that cellulose nanocrystals or other forms of cellulose fiber produced with a lower amount of sulfate groups on the surface could lead to better and more tailored compound properties.

Author contributions All authors contributed to the study conception and design. Material preparation, data collection and analysis were performed by Imiete Iikpoemugh Elo. The first draft of the manuscript was written by Imiete Iikpoemugh Elo and all authors commented on previous versions of the manuscript. All authors read and approved the final manuscript.

Funding Open access funding provided by Università degli Studi di Milano - Bicocca within the CRUI-CARE Agreement. The authors would like to acknowledge financial support of CORIMAV Pirelli.

Declarations

Conflict of interest The authors declare no competing interests.

References

Bai W, Li K (2009) Partial replacement of silica with microcrystalline cellulose in rubber composites. Compos Part A Appl Sci Manuf 40:1597–1605. https://doi.org/10.1016/j.compositesa.2009.07.006

Beyene D, Chae M, Dai J et al (2018) Characterization of cellulase-treated fibers and resulting cellulose nanocrystals generated through acid hydrolysis. Materials 11:1272. https://doi.org/10.3390/ma11081272

Bhattacharjee S (2016) DLS and zeta potential–What they are and what they are not? J Control Release 235:337–351. https://doi.org/10.1016/j.jconrel.2016.06.017

Boluk Y, Danumah C (2014) Analysis of cellulose nanocrystal rod lengths by dynamic light scattering and electron microscopy. J Nanoparticle Res 16:2174. https://doi.org/10.1007/s11051-013-2174-4

Börjesson M, Sahlin K, Bernin D, Westman G (2018) Increased thermal stability of nanocellulose composites by functionalization of the sulfate groups on cellulose nanocrystals with azetidinium ions. J Appl Polym Sci 135:45963. https://doi.org/10.1002/app.45963

Cao X, Xu C, Liu Y, Chen Y (2013) Preparation and properties of carboxylated styrene-butadiene rubber/cellulose nanocrystals composites. Carbohydr Polym 92:69–76. https://doi.org/10.1016/j.carbpol.2012.09.054

Cheng G, Varanasi P, Li C et al (2011) Transition of cellulose crystalline structure and surface morphology of biomass as a function of ionic liquid pretreatment and its relation to enzymatic hydrolysis. Biomacromol 12:933–941. https://doi.org/10.1021/bm101240z

Choi SS, Ko E (2014) Novel test method to estimate bound rubber formation of silica-filled solution styrene-butadiene rubber compounds. Polym Test 40:170–177. https://doi.org/10.1016/j.polymertesting.2014.09.003

Chollakup R, Suethao S, Suwanruji P et al (2021) Mechanical properties and dissipation energy of carbon black/rubber composites. Compos Adv Mater. https://doi.org/10.1177/26349833211005476

Colombo L, Zoia L, Violatto MB et al (2015) Organ distribution and bone tropism of cellulose nanocrystals in living mice. Biomacromol 16:2862–2871. https://doi.org/10.1021/acs.biomac.5b00805

Danon B, Görgens J (2015) Determining rubber composition of waste tyres using devolatilisation kinetics. Thermochim Acta 621:56–60. https://doi.org/10.1016/j.tca.2015.10.008

Dinand E, Vignon M, Chanzy H, Heux L (2002) Mercerization of primary wall cellulose and its implication for the conversion of cellulose I → cellulose II. Cellulose 9:7–18. https://doi.org/10.1023/A:1015877021688

Dong XM, Revol JF, Gray DG (1998) Effect of microcrystallite preparation conditions on the formation of colloid crystals of cellulose. Cellulose 5:19–32. https://doi.org/10.1023/A:1009260511939

Duchemin BJC (2015) Mercerisation of cellulose in aqueous NaOH at low concentrations. Green Chem 17:3941–3947. https://doi.org/10.1039/c5gc00563a

Dufresne A (2012) Nanocellulose: from nature to high performance tailored materials. Walter de Gruyter, Berlin. https://doi.org/10.1515/9783110254600

Dufresne A (2017) Cellulose nanomaterial reinforced polymer nanocomposites. Curr Opin Colloid Interface Sci 29:1–8. https://doi.org/10.1016/j.cocis.2017.01.004

Eyley S, Thielemans W (2014) Surface modification of cellulose nanocrystals. Nanoscale 6:7764–7779. https://doi.org/10.1039/c4nr01756k

Fernandesa IJ, Santos RV, Dos Santos ECA et al (2018) Replacement of commercial silica by rice husk ash in epoxy composites: a comparative analysis. Mater Res. https://doi.org/10.1590/1980-5373-MR-2016-0562

Fukahori Y (2005) New progress in the theory and model of carbon black reinforcement of elastomers. J Appl Polym Sci 95:60–67. https://doi.org/10.1002/app.20802

Gan PG, Sam ST, Abdullah MFB, Omar MF (2020) Thermal properties of nanocellulose-reinforced composites: a review. J Appl Polym Sci. https://doi.org/10.1002/app.48544

Gong J, Li J, Xu J et al (2017) Research on cellulose nanocrystals produced from cellulose sources with various polymorphs. RSC Adv 7:33486–33493. https://doi.org/10.1039/c7ra06222b

Gu J, Catchmark JM, Kaiser EQ, Archibald DD (2013) Quantification of cellulose nanowhiskers sulfate esterification levels. Carbohydr Polym 92:1809–1816. https://doi.org/10.1016/j.carbpol.2012.10.078

Habibi Y, Lucia LA, Rojas OJ (2010) Cellulose nanocrystals: chemistry, self-assembly, and applications. Chem Rev 110:3479–3500. https://doi.org/10.1021/cr900339w

Hasani M, Cranston ED, Westman G, Gray DG (2008) Cationic surface functionalization of cellulose nanocrystals. Soft Matter 4:2238–2244. https://doi.org/10.1039/b806789a

Haus R, Prinz S, Priess C (2012) Assessment of high purity quartz resources. In: Götze J, Möckel R (eds) Quartz: deposits, mineralogy and analytics, 1st edn. Springer, Berlin, Heidelberg, pp 29–51

Jacobs C, Müller RH (2002) Production and characterization of a budesonide nanosuspension for pulmonary administration. Pharm Res 19:189–194. https://doi.org/10.1023/A:1014276917363

Jordan JH, Easson MW, Condon BD (2019) Alkali hydrolysis of sulfated cellulose nanocrystals: optimization of reaction conditions and tailored surface charge. Nanomaterials 9:1232. https://doi.org/10.3390/nano9091232

Jorfi M, Foster EJ (2015) Recent advances in nanocellulose for biomedical applications. J Appl Polym Sci 132:n/a. https://doi.org/10.1002/app.41719

Kim JH, Shim BS, Kim HS et al (2015) Review of nanocellulose for sustainable future materials. Int J Precis Eng Manuf - Green Technol 2:197–213. https://doi.org/10.1007/s40684-015-0024-9

Klemm D, Kramer F, Moritz S et al (2011) Nanocelluloses: a new family of nature-based materials. Angew Chemie

- Int Ed 50:5438–5466. https://doi.org/10.1002/anie.201001273
Lin N, Dufresne A (2014) Surface chemistry, morphological analysis and properties of cellulose nanocrystals with gradiented sulfation degrees. Nanoscale 6:5384–5393. https://doi.org/10.1039/c3nr06761k
Llàcer Navarro S, Nakayama K, Idström A et al (2021) The effect of sulfate half-ester groups on cellulose nanocrystal periodate oxidation. Cellulose 28:9633–9644. https://doi.org/10.1007/s10570-021-04115-y
Mansikkamäki P, Lahtinen M, Rissanen K (2007) The conversion from cellulose I to cellulose II in NaOH mercerization performed in alcohol-water systems: an X-ray powder diffraction study. Carbohydr Polym 68:35–43. https://doi.org/10.1016/j.carbpol.2006.07.010
Michelin M, Gomes DG, Romaní A et al (2020) Nanocellulose production: exploring the enzymatic route and residues of pulp and paper industry. Molecules 25:3411. https://doi.org/10.3390/molecules25153411
Montes H, Chaussée T, Papon A et al (2010) Particles in model filled rubber: dispersion and mechanical properties. Eur Phys J E 31:263–268. https://doi.org/10.1140/epje/i2010-10570-x
Moon RJ, Martini A, Nairn J et al (2011) Cellulose nanomaterials review: structure, properties and nanocomposites. Chem Soc Rev 40:3941. https://doi.org/10.1039/c0cs00108b
Mostoni S, D'Arienzo M, Di Credico B et al (2021) Design of a Zn single-site curing activator for a more sustainable sulfur cross-link formation in rubber. Ind Eng Chem Res 60:10180–10192. https://doi.org/10.1021/acs.iecr.1c01580
Park S, Baker JO, Himmel ME et al (2010) Cellulose crystallinity index: measurement techniques and their impact on interpreting cellulase performance. Biotechnol Biofuels 3:1–10. https://doi.org/10.1186/1754-6834-3-10
Rajinipriya M, Nagalakshmaiah M, Robert M, Elkoun S (2018) Importance of agricultural and industrial waste in the field of nanocellulose and recent industrial developments of wood based nanocellulose: a review. ACS Sustain Chem Eng 6:2807–2828. https://doi.org/10.1021/acssuschemeng.7b03437
Rambo MKD, Ferreira MMC (2015) Determination of cellulose crystallinity of banana residues using near infrared spectroscopy and multivariate analysis. J Braz Chem Soc 26:1491–1499. https://doi.org/10.5935/0103-5053.20150118
Rodgers B, Waddell W (2013) The science of rubber compounding. In: Mark J, Erman B, Roland M (eds) The Science and Technology of Rubber, 3rd edn. Elsevier, pp 417–471
Roman M, Winter WT (2004) Effect of sulfate groups from sulfuric acid hydrolysis on the thermal degradation behavior of bacterial cellulose. Biomacromol 5:1671–1677. https://doi.org/10.1021/bm034519+
Rongpipi S, Ye D, Gomez ED, Gomez EW (2019) Progress and opportunities in the characterization of cellulose–An important regulator of cell wall growth and mechanics. Front. Plant Sci 9:1–28. https://doi.org/10.3389/fpls.2018.01894
Sienkiewicz M, Kucinska-Lipka J, Janik H, Balas A (2012) Progress in used tyres management in the European Union: a review. Waste Manag 32:1742–1751. https://doi.org/10.1016/j.wasman.2012.05.010
Tang WK, Neill WK (2007) Effect of flame retardants on pyrolysis and combustion of α-cellulose. J Polym Sci Part C Polym Symp 6:65–81. https://doi.org/10.1002/polc.5070060109
Ummartyotin S, Manuspiya H (2015) A critical review on cellulose: from fundamental to an approach on sensor technology. Renew Sustain Energy Rev 41:402–412. https://doi.org/10.1016/j.rser.2014.08.050
Vanderfleet OM, Reid MS, Bras J et al (2019) Insight into thermal stability of cellulose nanocrystals from new hydrolysis methods with acid blends. Cellulose 26:507–528. https://doi.org/10.1007/s10570-018-2175-7
Voronova MI, Surov OV, Zakharov AG (2013) Nanocrystalline cellulose with various contents of sulfate groups. Carbohydr Polym 98:465–469. https://doi.org/10.1016/j.carbpol.2013.06.004
Yao W, Weng Y, Catchmark J (2020) Improved cellulose X-Ray diffraction analysis using fourier series modeling. Cellulose 27:5563–5579. https://doi.org/10.1007/s10570-020-03177-8
Yasir HA, Maamori MH, Al, Ali HM (2015) Effect of carbon black types on curing behavior of natural rubber. J Adv Eng Technol 2:77–80
Zhao Y, Zhang Y, Lindström ME, Li J (2015) Tunicate cellulose nanocrystals: preparation, neat films and nanocomposite films with glucomannans. Carbohydr Polym 117:286–296. https://doi.org/10.1016/j.carbpol.2014.09.020
Zoia L, Morelli A, Talamini L et al (2020) Cellulose nanocrystals: a multimodal tool to enhance the targeted drug delivery against bone disorders. Nanomedicine 15:2271. https://doi.org/10.2217/nnm-2020-0139
Zoppe JO, Johansson LS, Seppälä J (2015) Manipulation of cellulose nanocrystal surface sulfate groups toward biomimetic nanostructures in aqueous media. Carbohydr Polym 126:23–31. https://doi.org/10.1016/j.carbpol.2015.03.005